# CoNiCrAlY microstructural changes induced during Cold Gas Dynamic Spraying

P. Richer [a,*], A. Zúñiga [b], M. Yandouzi [a], B. Jodoin [a]

[a] University of Ottawa, Ottawa, Ontario, Canada
[b] Department of Mechanical Engineering, University of Chile, Beauchef 850, Santiago, Chile

*Keywords:*
Nanocrystalline
Cold spray
MCrAlY
TEM
Plastic deformation

A B S T R A C T

The present study is part of an ongoing research project that aims to develop high performance bond coats by means of Cold Gas Dynamic Spraying (CGDS) for the manufacturing of thermal barrier coatings (TBC). The objective of this work is to investigate the microstructure of a CGDS coating and compare it to that of the original feedstock powder in order to determine whether any microstructural changes have occurred during the deposition process. CoNiCrAlY coatings were deposited using the CGDS system developed at the University of Ottawa Cold Spray Laboratory. Scanning electron microscopy, transmission electron microscopy and X-ray diffraction techniques were used to assess the phases and microstructure of the original feedstock powder and coatings produced. Contrarily to the generally accepted theory that the CGDS process does not lead to changes in the deposited material's microstructure and phase, results from the analysis performed in this study demonstrate the occurrence of important microstructural and phase changes. Evidence of grain refinement of the γ-phase matrix down to the nanometre scale as well as partial dissolution of β-phase precipitates was observed. It is believed that these changes are attributed to the severe plastic deformation encountered by the deposited particles.

## 1. Introduction

The Cold Gas Dynamic Spraying (CGDS) process, which has undergone its early developments in Russia [1], has been the object of worldwide interest over the last decade with the number of peer reviewed journal papers and patents published on the topic growing almost exponentially [2–20]. After several years of research and development activities on the topic, many commercial systems have emerged and are now available from many equipment manufacturers in various forms, mainly categorized as low-pressure and high-pressure systems [2] while many in-house systems have been developed and used by various academic laboratories to pursue fundamental and explorative works on the process [3–5]. This latest coating technology has already found some industrial applications and it is expected that more targeted applications will be developed as numerous development projects are currently underway worldwide [6–8]. In the CGDS process, solid particles of size range characteristically between 10 and 50 μm are accelerated in a supersonic inert gas flow (usually nitrogen or helium, although air can also be used) and directed towards the object to be coated [1]. When the particles impact the object at a velocity higher than the material dependant critical velocity, they plastically deform and adhere to the substrate or to the already deposited layer of material through what is believed to be primarily mechanical interlocking [9].

Over the last decade, several studies have reported that a wide variety of materials have successfully been sprayed using the CGDS process, such as pure metals [10–13], alloys in conventional [14,15], nanocrystalline [3,16,17] and amorphous [18] forms as well as cermets in conventional and nanocrystalline forms [4,19] and metal–matrix composites [20]. The main coating characteristics observed and reported in these studies were: 1) low porosity level attributed to sufficient plastic deformation experienced by the particles upon impact on the substrate and subsequent densification caused by impinging particles on the existing coating [10]; 2) absence of oxidation due to the use of inert propellant gases and/or the use of relatively low gas temperature [1]; 3) good adherence between the substrate and the coatings attributed to sufficient plastic deformation of the sprayed particles upon impact with the substrate [21]; 4) increased hardness compared to the original feedstock powder as a result of the cold working effect on the original feedstock powder [22] and 5) absence of chemical and microstructural changes compared to the feedstock powder attributed to the inert and low temperature environment/propellant gas involved in the process [1,3,17].

Many studies have also reported modelling efforts specifically directed at improving the understanding of the particle/substrate and particle/particle impact phenomena [23]. Although it is reported that more work needs to be done in this area in order to fully understand the

* Corresponding author. Department of Mechanical Engineering, Faculty of Engineering, University of Ottawa, 770 King Edward Avenue, Ottawa, Ontario, Canada K1N 6N5. Tel.: +1 613 562 5800x2474; fax: +1 613 562 5177.
*E-mail address:* prich097@uottawa.ca (P. Richer).

**Table 1**
Chemical composition of the AMDRY 9951 CoNiCrAlY powder

| Element | Co | Ni | Cr | Al | Y |
|---|---|---|---|---|---|
| Wt.% | 37.97 | 32.01 | 21.22 | 8.04 | 0.5 |

impact/deformation physical mechanisms, there is a general consensus on the deformation process occurring locally at the particle boundaries during impact, which is referred to as adiabatic shear instability. It is expected that this deformation mechanism promotes intimate contact between the particle and the substrate and between two adjacent particles. The adiabatic shear instability mechanism was originally described in details by Wright [24] and subsequently used to explain the deformation mechanism for particle/particle and particle/substrate bonding during the CGDS process [9,25]. The assumption that the particle/particle or particle/substrate interaction is adiabatic is based on the fact that the thermal diffusion distance is small during the short contact time during impact [9], thus allowing to neglect heat conduction during the particle impact and deformation. As a result, the plastic strain energy dissipated in the form of heat results in a localized temperature increase at the particle boundary. This in turn causes material softening as well as possible shear localization (adiabatic shear instability) that facilitates the plastic deformation and interlocking of splats, each particle thus conformably shaping to the previous layer producing a dense coating. Modelling results have revealed that the localized heat dissipation at the particles boundaries can result in a temperature increase capable of causing localized melting, helping the creation of intimate contact between clean surfaces and promoting metallurgical bonding at the particle/particle surfaces [23,26].

These predicted localized melting and metallurgical bonding phenomenon contradict what is generally observed and presented as key features of CGDS coatings. As mentioned previously, the bonding mechanism is said to be due mainly to mechanical interlocking and the process does not lead to any chemical and microstructural changes. Since little experimental evidence of true metallurgical bonding between particles has been presented [21] and thus no true demonstration that localized melting does generally occur, the complete validity of the models predictions is yet to be demonstrated. This suggests that some relevant physical phenomenon might have been omitted in the models.

The present study is part of an ongoing research project that aims to develop high performance bond coats by means of CGDS for the manufacturing of thermal barrier coatings (TBC) to be applied on hot components of gas turbine engines. The performance and durability of a TBC has been shown to be directly linked to the bond coat properties, more specifically its microstructure and oxidation behaviour [27]. Complete control of the bond coat material microstructure throughout the deposition process is desirable as it allows for the optimisation of the coating's oxidation resistance and ultimately the improvement of TBC performance. CGDS has demonstrated much promise in preserving a material's microstructure throughout the deposition process [3,17], and has therefore been selected in this ongoing research project as the preferred deposition technique for bond coats. Conversely, changes in a material's microstructure resulting from the high-velocity impact of particles during the CGDS process has also been observed [13,28]. As such, the objective of the work presented in this paper is to perform a detailed investigation of CGDS bond coats in order to assess any changes in the microstructure of the coatings compared to the original feedstock powder. In particular, scanning electron microscopy, transmission electron microscopy and X-ray diffraction techniques are used to assess the phases and microstructure of the original feedstock powder and coatings produced. The feedstock material chosen for this work is a commercially available CoNiCrAlY powder commonly used in the industry for the manufacturing of bond coats.

## 2. Experimental set-up

### 2.1. Feedstock material

The feedstock powder considered in this study is the gas atomized AMDRY 9951 (Sulzer Metco). It is a conventional CoNiCrAlY powder with a spherical morphology and a particle size distribution ranging from 5 to 37 μm (according to powder specifications), thus making it generally suitable for the CGDS process. The chemical composition of this powder is presented in Table 1. It is generally used in high temperature applications such as bond coatings for TBCs where oxidation and hot-corrosion are problematic.

### 2.2. Cold Gas Dynamic Spray facility

The CoNiCrAlY coating samples were produced using the CGDS system developed at the University of Ottawa Cold Spray Laboratory [3]. The system consists of a computer controlled high-pressure primary gas supply used for the main propellant flow as well as a secondary lower pressure gas supply used as the feedstock powder carrier flow. The main gas is fed through an electric gas heater capable of producing gas temperatures up to 700 °C, and is then redirected through a converging/diverging nozzle to generate the supersonic flow. The carrier gas is connected to a commercially available powder feeder (Praxair, model 1264) and entrains the powder particles into the main flow. The substrate holder is mounted on a motorized X–Y traverse system equipped with a computer controlled variable velocity positioning system. More details on the spraying system can be found elsewhere [3]. For the present study, helium was used for both the main propellant and carrier gases. The propellant gas pressure and temperature were set at 1.0 MPa and 550 °C respectively at the nozzle inlet. Coatings were manufactured in a single pass onto grit blasted aluminum 6061 alloy substrates.

### 2.3. Particle velocity, feedstock powder and coating characterization

Particle velocities at the spray nozzle exit were measured using a laser in-flight diagnostic system; a Cold Spray Meter (Tecnar Automation Ltd., St-Bruno, Québec, Canada). While a continuous laser illuminates a measurement volume, a dual-slit photomask captures the signal generated by individual particles passing in front of the sensor. The signal from the photo sensor is amplified, filtered and analyzed. In-flight diagnostic of each individual particle that crosses the measurement volume is performed by determining the time between the two peaks of the particle signal. Particle velocities are then obtained by dividing the known distance between the two-slits by their time of flight. The velocity measurements were taken at a point 5 mm from the spraying gun exit, without the presence of a substrate.

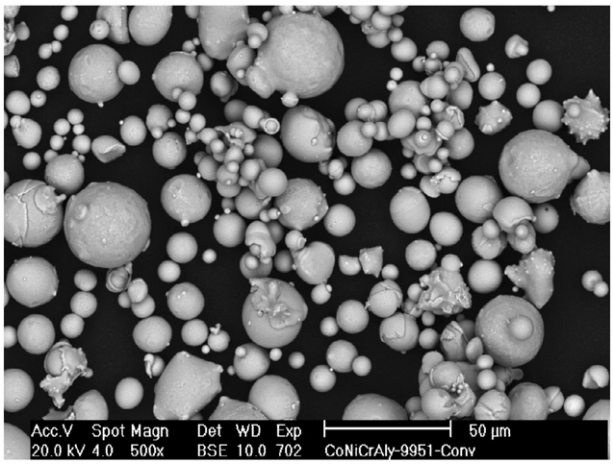


**Fig. 1.** SEM image of as-received CoNiCrAlY powder.

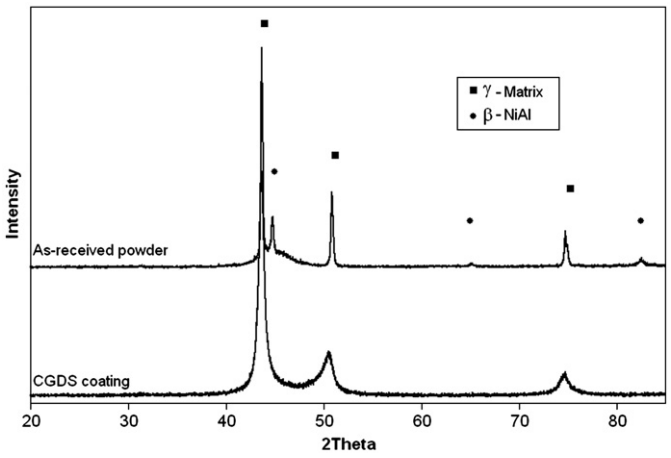


**Fig. 2.** XRD spectra of as-received CoNiCrAlY powder and as-deposited CGDS coating.

Phase identification for the feedstock powder and coatings was performed by X-ray diffraction (XRD). The XRD analyses were carried out with a Philips X-Pert model PW 1830 generator diffractometer with CuKα (λ = 0.15406 nm) radiation. Detailed scans with step size of 0.01° and step time of 2 s were conducted with 2$\theta$ values ranging from 20° to 85°.

Microstructural characterization of the feedstock powder and coatings was performed by scanning electron microscopy using a Philips XL 30, LaB6 analytical SEM. The powder samples were examined directly. Prior to microstructural observations, cross-sections of the coatings were obtained by resin cold mounting followed by grinding and polishing to a 0.05 μm surface finish. The porosity of the coating layers was measured using an optical microscope (Olympus Metallurgical Microscope), 400× magnification images and image analysis software (Clemex Vision-Lite). The intensity range and thresholds were standardized on reference materials, and ten measurements were performed per sample, at various positions within the coating structure.

Microstructural investigation was also performed using a transmission electron microscopy (TEM), FEI Tecnai-G2 F20 microscope operating at 200 kV. Prior to TEM observation the powder samples were cold mounted in epoxy followed by grinding, polishing, and ion milling.

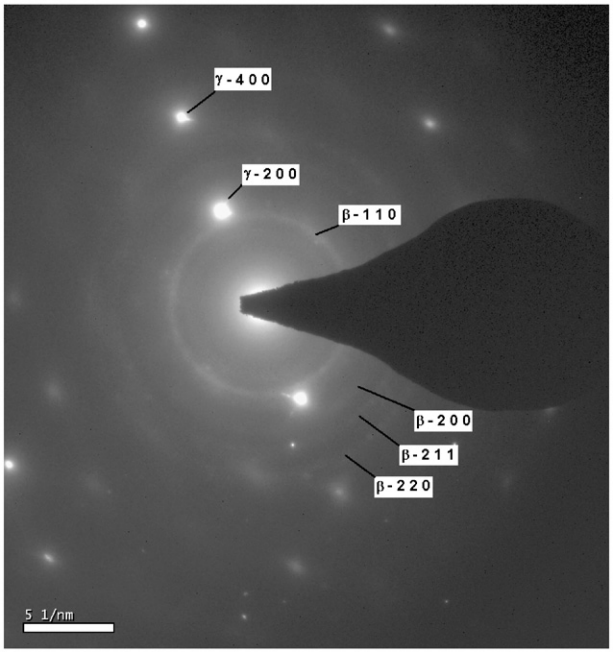


**Fig. 3.** SAED pattern of as-received CoNiCrAlY powder.

The coating samples were prepared by removing the substrate by sanding, followed by dimpling and ion milling. Different modes of observation were used; in particular, bright field (BF) and dark field (DF) modes as well as Selected Area Electron Diffraction (SAED) for phase identification.

## 3. Results and discussion

### 3.1. Powder Characterization

The morphology of the as-received CoNiCrAlY powder is shown in Fig. 1. As can be seen from this figure, the powder has a spherical morphology and the size of the particles falls within the specified range of 5–37 μm. Fig. 2 shows the XRD spectra of the as-received CoNiCrAlY powder. Phase identification shows the presence of a dominant phase represented by three strong peaks associated to the (1 1 1), (2 0 0) and (2 2 0) atomic planes. This phase corresponds to a fcc γ-matrix consisting of a Co–Ni–Cr solid solution. The presence of a second phase

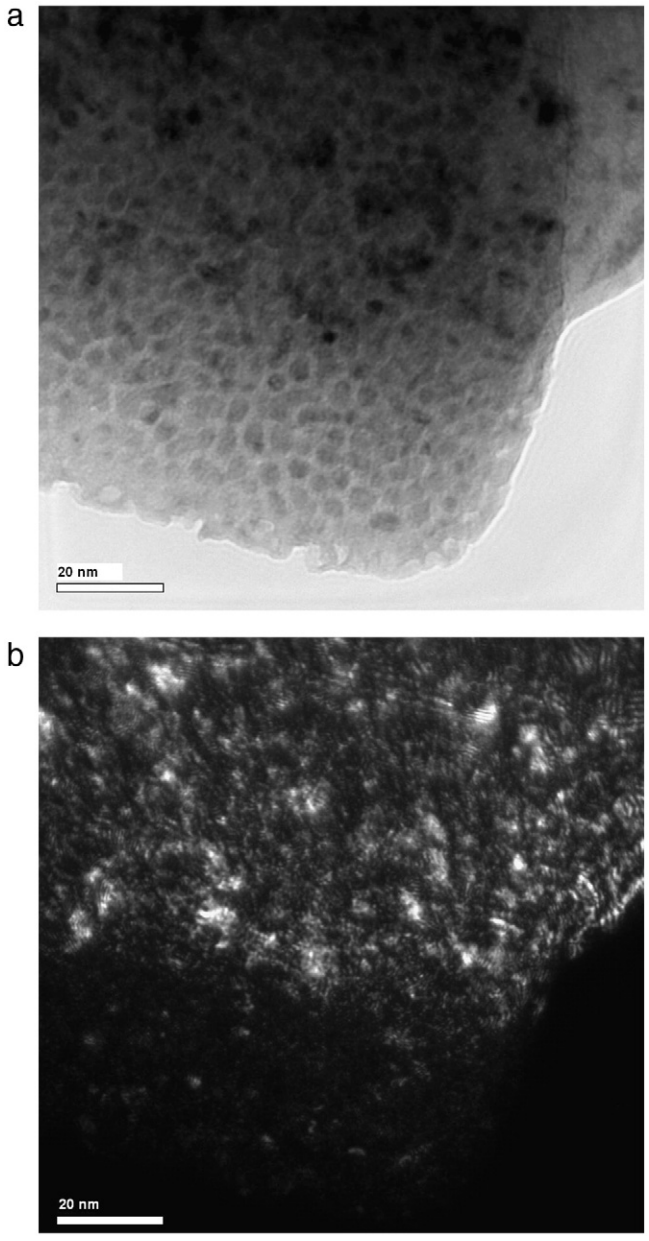


**Fig. 4.** Bright field (top) and dark field (bottom) TEM images of the as-received CoNiCrAlY powder.

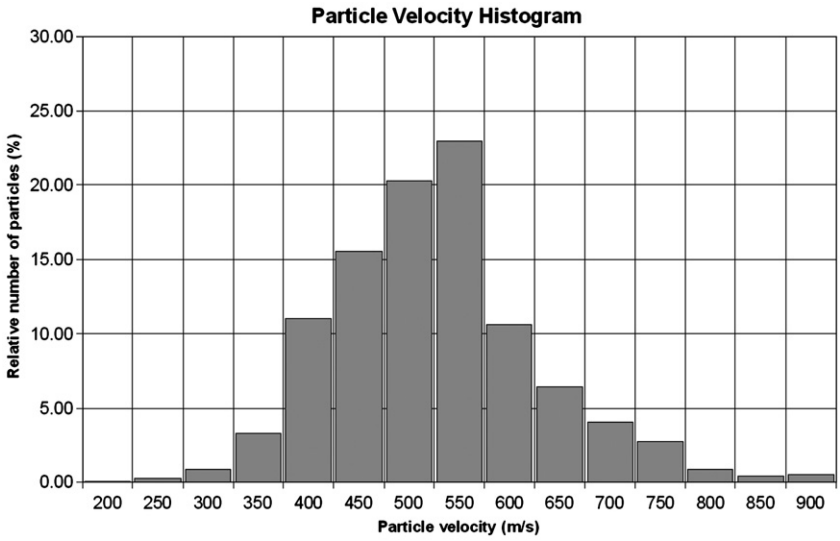


**Fig. 5.** Particle velocity distribution during CGDS deposition.

characterized with weaker peaks can also be observed and is identified as a NiAl bcc β-phase. The presence of a small "hump" underneath the largest β-phase peak is also observed. This is believed to be attributed to the presence of some amorphous phase content in the as-received feedstock powder. Given that this powder was produced by spray atomization, a process known to lead to fast particle solidification and high cooling rates [29], it is rationalized that in the case of very fine particles (smaller diameters), spray atomization can possibly lead to amorphous microstructures. To confirm this, an XRD scan of as-received AMDRY 9954 powder was conducted and did not reveal the presence of such an amorphous hump. The AMDRY 9954 powder has the same chemical composition as the AMDRY 9951 powder, however its particle size distribution is different: the latter is finer with particle diameters of 5–37 μm, while the former is coarser with a particle size range of 16–64 μm. This tends to confirm that the very fine particles in the 9951 powder, notably those with diameters between 5 and 16 μm, would have some amorphous microstructure.

Fig. 3 presents the SAED pattern of the as-received CoNiCrAlY feedstock powder. It was identified that the strong diffraction spots correspond to the (2 0 0) and (4 0 0) γ-phase. This diffraction pattern suggests that the powder is likely polycrystalline and composed of microsized γ-phase grains. It should also be noted that ordering spots were observed thus confirming the solid solution (Co–Ni–Cr) of the matrix. Ring-shaped diffraction patterns are also observed and reveal the presence of a β phase. These rings are identified to be (2 0 0), (2 1 1) and (2 2 0) β-NiAl. The ring-like shape of this diffraction pattern indicates a fine grain size, therefore suggesting the presence of fine precipitates of the β-NiAl phase within the γ-matrix. The presence of both the γ and β phases in the diffraction pattern confirms the results obtained from the XRD analysis. Conversely, the presence of amorphous microstructure is not visible in the diffraction pattern of Fig. 3. This is likely attributed to high intensity associated to the crystalline structures, hindering the observation of the amorphous halo in the diffraction pattern.

Fig. 4 shows (a) BF and (b) DF TEM images of the as-received feedstock CoNiCrAlY powder. The images confirm the presence of very fine grained precipitates (β-NiAl) embedded in the γ-matrix. These β-phase precipitates were determined to have a spherical morphology and grain sizes ranging from 3 to 5 nm.

### 3.2. Particle velocity characterization

Particle velocity measurements were carried out prior to spraying the coatings to obtain the in-flight particle velocity distributions of the feedstock powders. The particle velocity distribution obtained is presented in Fig. 5. The particle velocities range from 250 to 900 m/s, with an average velocity of 558 ± 95 m/s. This average particle velocity appears to be low when compared to critical velocities usually found

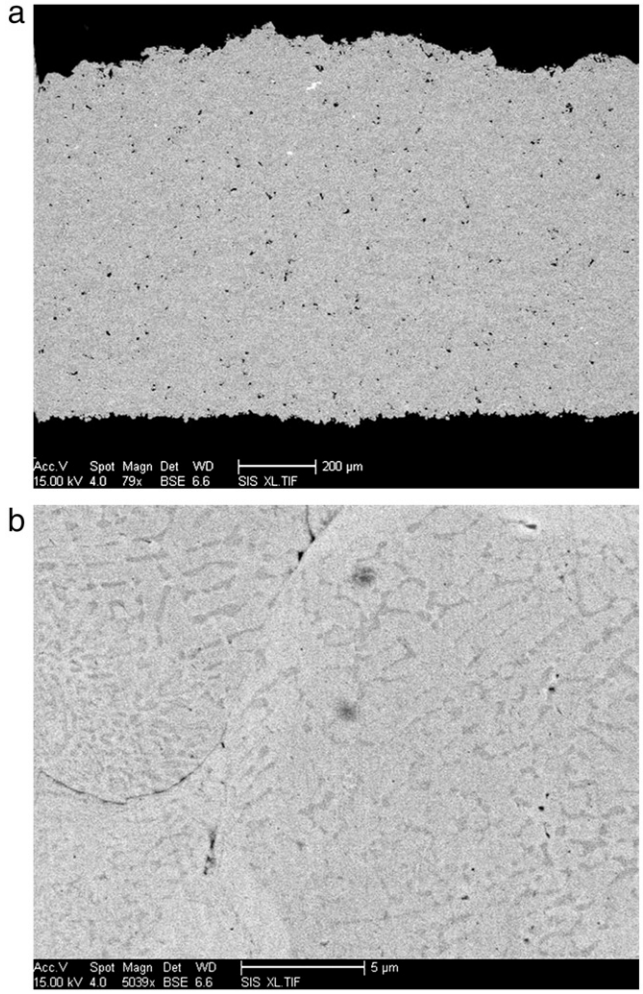


**Fig. 6.** Backscattered electron mode images of CoNiCrAlY coatings at different magnifications.

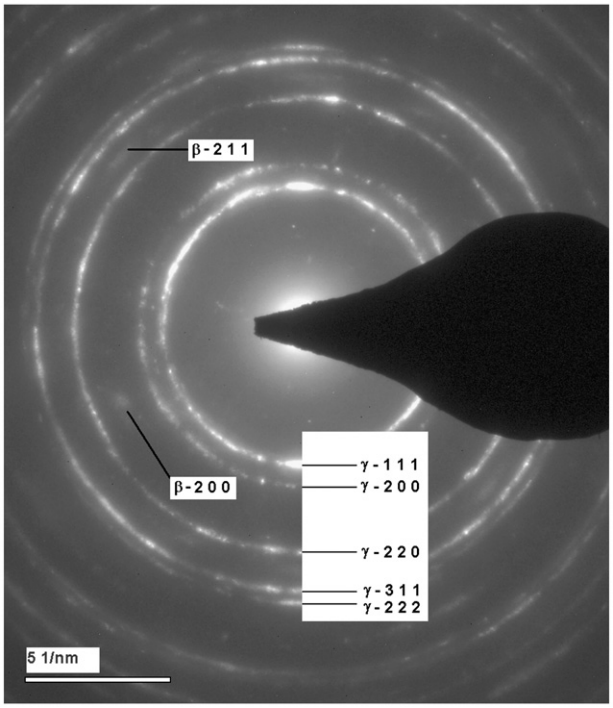


**Fig. 7.** SAED pattern of the as-sprayed CoNiCrAlY CGDS coating.

in the literature [23,25,26], especially for nickel-based particles. As such, it is expected that the coatings produced will likely be porous as a result of reduced particle deformation upon impact and that the deposition efficiency will be low compared to typical deposition efficiency of other softer materials deposited using the CGDS process. It is also expected that only the smallest particles, which are likely to achieve the fastest impact velocities for aerodynamic considerations [30] will deform sufficiently upon impact with the substrate to form the coatings. Higher particle impact velocities could be obtained using the same nozzle if the gas stagnation pressure was increased in order to enhance the propellant gas–feedstock particle momentum transfer. However, the powder feeder used in this study limits the maximum operating pressure within the system and it was thus impossible to achieve higher particle velocities.

### *3.3. Coatings characterization*

Fig. 6 shows backscattered electron mode SEM images of the as-sprayed CoNiCrAlY coatings produced using the CGDS process. As can be observed in Fig. 6a, the powder was successfully deposited and sufficient build-up of the coating led to a thickness of approximately 800 μm. The coating also exhibits a low level of porosity and interlamellar crack content. The percentage area porosity was evaluated at less than 2%, which might be surprising considering the fact that Ni-based powders have a relatively high critical velocity. The low porosity content is mostly attributed to the compaction effect caused by the particle impingement, thus promoting the formation of a thick and dense coating, as reported in previous studies [3,10,13]. To promote this compaction effect during the coating deposition, a low nozzle traversing speed was used, thus allowing a given area of the coating to be exposed to the incoming jet of particles for a longer period of time. As can be seen in Fig. 6b, there appears to be no evidence of metallurgical bonding between the particles, which is attributed to insufficient kinetic energy available upon impact to cause this phenomenon to happen. This suggests that the coating integrity is attributed solely to mechanical interlocking of the deposited particles.

Fig. 2 also shows the XRD scan of the as-sprayed conventional CoNiCrAlY coating. When compared to the XRD spectrum of the as-received feedstock powder, significant differences can be observed. The first important observation is that peak broadening has occurred for the γ-peaks which could be attributed to grain refinement and/or induced micro-stresses caused by the deposition process. A second observation is that the peaks associated to the β-phase are no longer distinguishable, which may once again be the result of grain refinement of this phase, thus leading to peak broadening and reduced diffraction intensity. However, given the very fine grain size of the β-phase precipitates in the original feedstock powder and the apparent absence of β peaks in the resulting CGDS coating, it is possible that this phase may have dissolved into the γ-matrix. The differences between the two XRD spectra demonstrate that the CGDS deposition process has had an effect on the material microstructure, as opposed to what is usually advertised as potential benefits of the CGDS process.

In order to better assess the as-sprayed coating's microstructure and to gain a clearer understanding of its behaviour upon deposition, a TEM analysis was carried out. Fig. 7 shows the diffraction pattern of the as-

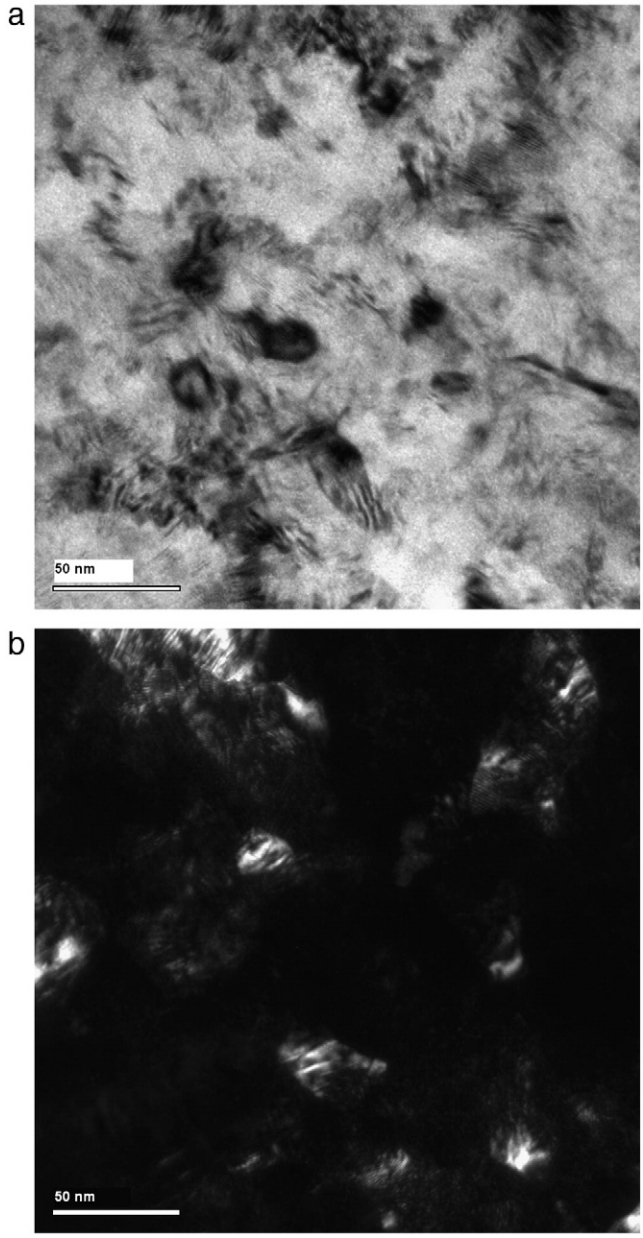


**Fig. 8.** Bright field (top) and dark field (bottom) TEM images of the as-sprayed CoNiCrAlY CGDS coating.

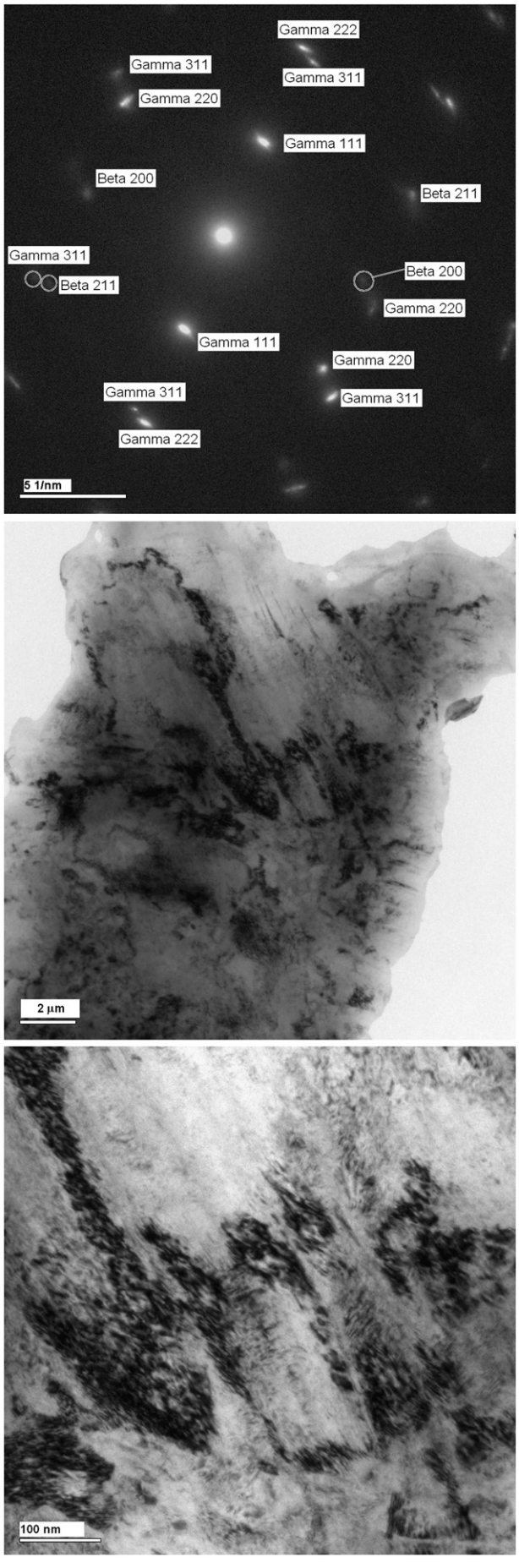


sprayed CoNiCrAlY coating. This diffraction pattern is considerably different to that of the original feedstock powder as it clearly reveals multiple diffractions rings associated to the γ-phase Co–Ni–Cr solid solution. The presence of these diffraction rings as opposed to diffraction spots (as were observed in the as-received powder diffraction pattern) demonstrates that the grains in the γ-matrix have undergone considerable refinement. Smaller ring fragments can also be observed (although they are faint) and are attributed to diffractions of β-phase precipitates. These β-phase diffractions are much weaker than those obtained with the as-received powder, thus suggesting a lower β-phase content in the coating when compared to the original powder. These results are in accordance with the XRD analysis, further confirming that grain refinement of the γ-phase and some level of dissolution of the β-phase has occurred during the CGDS deposition process. Fig. 8 shows bright field and dark field TEM images of the same as-sprayed coating. These images confirm that in this area of the coating, the microstructure is composed of some fine γ-phase grains of approximately 20–30 nm in diameter. Alternatively, γ-phase grains of approximately 100–200 nm in diameter were also found in other regions of the coating, as shown in the TEM images from Fig. 9. Further analysis confirmed the existence of a bimodal grain size distribution for the γ-matrix in the CGDS coating, thus revealing that refinement of the γ-matrix grains is not uniform throughout the coating.

### 3.4. γ-Phase grain refinement process

The XRD and TEM analyses performed on the as-received powder and as-sprayed coating revealed that the γ-matrix underwent grain refinement during the CGDS deposition process. Given the absence of significant heating of the particles in CGDS as well as the use of inert gases in the process, it is expected that changes in the microstructure be solely caused by the intense plastic deformation of the sprayed material upon deposition. Grain refinement resulting from severe plastic deformation is a well known phenomenon that has been studied and applied extensively [31,32]. In fact, the process of subjecting materials to severe plastic deformation has been shown to be one of many effective methods for producing nanocrystalline materials [33–35]. Processes such as high-pressure torsion and equal-channel angular pressing have been used for the production of bulk nanocrystalline solids [34], whereas mechanical milling and alloying has been used for the synthesis of nanocrystalline particles [35,36]. In mechanical milling, the plastic deformation of the milled material occurs as particles are crushed by the larger fast-moving grinding media particles. The nature of plastic deformation in mechanical milling is thus attributed to the impact of the powder particles with the higher momentum grinding media, and therefore it can be envisioned that it is not extensively different to the plastic deformation mechanism of powder particles deposited during the CGDS technique. To further verify this, a portion of the as-received CoNiCrAlY feedstock powder was subjected to mechanical milling in order to produce nanocrystalline CoNiCrAlY feedstock particles. The powder was mechanically milled for 8 h at 200 rpm under a constant supply of liquid nitrogen in an Attritor Union Process 01-HD Szegvari mill. Stainless steel 440 balls (4.8 mm in diameter) were used as the grinding media with a ball-to-powder weight ratio of 24:1. This process is often referred to as cryomilling and has been shown to be one of many successful processes used to produce materials with nanocrystalline microstructures [33]. Fig. 10 presents the XRD spectra of the cryomilled powder and the conventional CGDS coating. Comparison of these spectra shows that the cryomilled powder and CGDS coating have a similar microstructure. When compared to the spectrum of the original feedstock powder, both these spectra show the occurrence of peak broadening of the γ-matrix, as well as the attenuation/disappearance of the peaks associated to the β-phase. Discrepancy with respect to

**Fig. 9.** SAED pattern and bright field TEM images of the as-sprayed CoNiCrAlY CGDS coating.

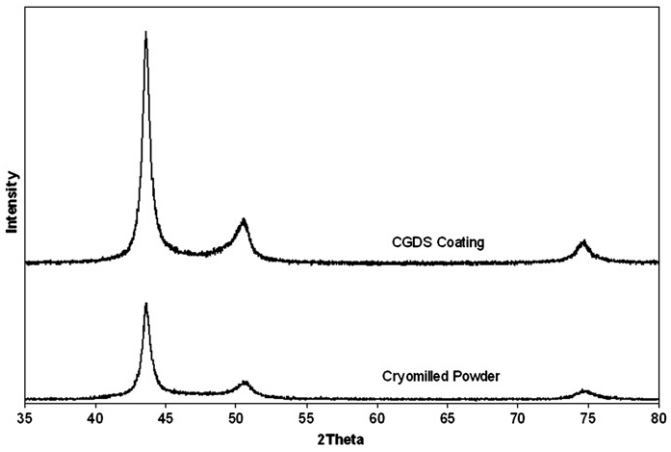


**Fig. 10.** XRD spectra of as-cryomilled CoNiCrAlY powder and as-sprayed CGDS coating.

spectrum intensity between the two scans is attributed to the different physical condition of the samples (powder form and solid form for the cryomilled powder and CGDS coating sample respectively). These findings seem to demonstrate that the impact of powder particles on the substrate during the CGDS process is similar to plastic deformation in a material caused by mechanical milling, thus leading to similar microstructural evolutions in the material. It is therefore hypothesized that the concepts and mechanisms of grain refinement and phase transformations/dissolution observed in a material subjected to mechanical milling (severe plastic deformation) can thus be extended to explain the behaviour of a material deposited by CGDS.

Suryanarayana [36] explained that grain refinement and the mechanism of formation of nanostructures in mechanical milling initiates from the formation of shear bands resulting from the high deformation rates encountered in mechanical milling. These shear bands have a high dislocation density, and with continued milling time, the increasing dislocation density leads to higher atomic level strains. When a given dislocation density is reached in the highly strained region, the crystal breaks down into smaller subgrains separated by low-angle grain boundaries, resulting in a decrease of the lattice strain. As milling continues and the material undergoes further plastic deformation, shear bands form in areas that were previously unstrained. As this process continues to happen, grain sizes steadily decrease and the shear bands coalesce. The low-angle grain boundaries are replaced by higher angle grain boundaries, thus implying grain rotation. The result is the formation of dislocation-free nanocrystalline grains with random orientations. This grain refinement mechanism can also be used to explain the reduction of the grain size of the γ-phase in the CoNiCrAlY during the CGDS deposition process. In CGDS, shear bands are formed at the particle/substrate and particle/particle interfaces [9,25] as a result of the high deformation rates encountered upon impact, thus allowing the grain refinement mechanism to be initiated. The impingement from the subsequent impacting particles provides additional plastic deformation of the sprayed material, therefore introducing additional shear bands and dislocations and assisting the grain refinement process. Since the evolution of plastic deformation in CGDS coatings is restricted to the short exposure time of the coating under the impinging jet of particles, it is expected that grain refinement in the CGDS coating material would be less significant than in a mechanically milled material. Mechanical milling is typically carried out for numerous hours, which ensures that the material has been uniformly plastically deformed and that grain refinement has been achieved equally throughout the material. This is not the case for CGDS coatings: different extents of plastic deformation are undergone by the impacting particles due to the varying particle impact velocities (and consequently impact force) from one particle to the next. Additionally, different degrees of plastic deformation within various regions of a single particle exist due to the formation of shear bands upon impact. These varying levels of plastic deformation in the deposited material explain the reason for the existence of a bimodal γ-phase grain size distribution in the CGDS coating. It is believed that the particles that achieve a greater impact velocity will undergo a more important reduction in grain size. Also, the regions of the particles having undergone the most plastic deformation upon deposition (shear bands at the impacting surfaces) will likely experience more significant grain refinement, as suggested in Fig. 8 by the existence of 20–30 nm γ-phase grains. Conversely, central regions of larger particles with lower impact velocities are expected to encounter less plastic deformation and will experience little or no grain refinement, as observed in Fig. 9 by the presence of 100–200 nm grains. Observation of the BF images in Figs. 8 and 9 further validates the similarities in the grain refinement mechanisms observed in mechanical milling and in CGDS. Fig. 9 shows the presence of grains separated by low-angle grain boundaries, thus suggesting that the grain refinement process has been initiated but the level of plastic deformation in this area of the coating is insufficient to cause further refinement or grain rotation. Conversely, Fig. 8 shows fine grains with high-angle grain boundaries, which suggests that this area of the coating has been subjected to enough plastic deformation to cause substantial grain refinement and grain rotation. As such, areas in the coating subjected to less plastic deformation will exhibit limited grain refinement, resulting in coarser grains with low-angle grain boundaries, whereas areas subjected to more plastic deformation will exhibit increased grain refinement, leading to fine grains with high-angle grain boundaries. It was not possible to verify specifically which areas of the coating had undergone more grain refinement based on the TEM analysis performed in the present study. However, the level of grain refinement is believed to be directly linked to the extent of plastic deformation as discussed previously. Investigation of the different extents of grain refinement as a function of various regions of a deposited coating will be the focus of a future study.

### 3.5. β-Phase dissolution process

The XRD and TEM investigations of the as-received powder and as-sprayed coating also revealed transformations of the β-phase. Results suggest that the fine β-phase precipitates in the sprayed material undergo a dissolution process into the γ-matrix during CGDS deposition. Once again, it is believed that this type of microstructural evolution is the result of intense plastic deformation encountered by the sprayed material throughout the CGDS process. Phase transformations and

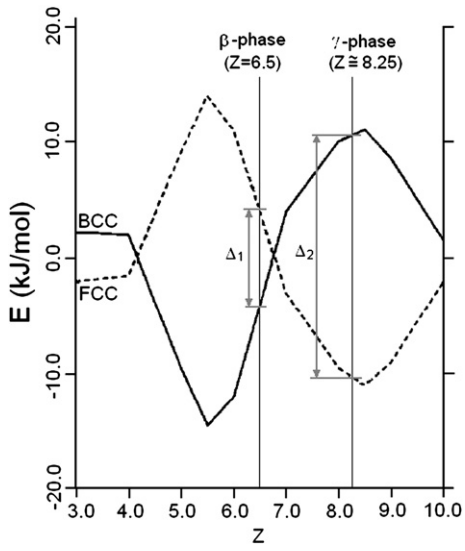


**Fig. 11.** Lattice stability as a function of the average number of valence electrons per atom ($Z$) for two types of crystal structure: bcc (solid curve) and fcc (dashed curve) (adapted from [37]).

dissolution resulting from severe plastic deformation have been observed elsewhere [32,37], and the occurrence of deformation driven dissolution of the β-phase during the CGDS process would explain the results observed in this study. Dissolution of the intermetallic β-phase in the CoNiCrAlY alloy due to severe plastic deformation is believed to be attributed to instabilities in the crystal lattice because of its high strain levels and energy state. Similarly to the grain refinement mechanism, the severe plastic deformation of the sprayed particles leads to high dislocation densities in the material, resulting in high average strains at the atomic level. This increased energy state within the material can compromise the stability of the crystal lattice. Upon increased energy and strain levels, it becomes energetically favourable for the crystal structure to change in order to better accommodate the energy and strain levels. As discussed previously, this may be done by breaking down larger grains into finer subgrains, which eventually results in grain refinement. However, if the grains are already very fine (as is the case for the β-phase in this study), the process of grain refinement reaches a limit and is no longer favourable. Changes in the crystal lattice structure itself may then occur. Fig. 11 shows the lattice stability as a function of the average valence electrons per atom ($Z$) for two common crystal structures (adapted from [38]). The β-phase was shown to be composed of NiAl which has an average number of valence electrons per atom of $Z$=6.5. According to Fig. 11, this intermetallic naturally forms as a bcc crystal lattice at equilibrium since this is the crystal structure that has the lowest energy state for the given average number of valence electrons per atom. Conversely, the γ-phase was shown to consist of a Co–Ni–Cr solid solution with an fcc lattice structure for which the average number of valence electrons per atom is $Z$=8.25. According to Fig. 11, this phase would likely form as an fcc crystal lattice at equilibrium. These observations are in accordance with the findings and results presented in this study. Fig. 11 also shows that the bcc NiAl β-phase observed in the CoNiCrAlY material is less stable than its fcc γ-matrix Co–Ni–Cr solid solution counterpart. It can be observed that an energy increase equal to $\Delta_1$ (~7.1 kJ/mol) in the β-phase bcc lattice would be sufficient to favour a crystal lattice transformation from bcc to fcc. Alternatively, an energy increase equal to $\Delta_2$ (~21.4 kJ/mol) in the γ-phase fcc lattice would be required to favour the transformation of the fcc crystal structure to bcc. The high-velocity impact of the sprayed particles results in a large energy increase in the deposited material, which is seemingly sufficient to cause dissolution of the bcc β-phase into the fcc matrix, but not sufficient to cause transformation of the fcc matrix into a bcc lattice structure. This is attributed to the fact that the large γ-matrix grains absorb a significant amount of energy during the plastic deformation and grain refinement processes, whereas the initially fine β-precipitates cannot undergo the same extent of deformation or refinement. It is therefore apparent that the initial fine grain structure of the β-precipitates and their relative lattice instability when compared to the fcc γ-matrix are two factors that tend to favour the deformation-driven dissolution process.

## 4. Conclusion

CoNiCrAlY bond coats were successfully deposited using the CGDS apparatus developed at the University of Ottawa Cold Spray Laboratory. Coatings were characterized as having low porosity (<2%) and large build-up thickness up to 800 μm. Velocity measurements yielded an average particle velocity of 558±95 m/s, which is somewhat low compared to predicted critical velocities for Ni-based alloys. As such, coating build-up and compaction was mostly attributed to particle impingement and bonding was found to be predominantly caused by mechanical interlocking. XRD and TEM investigations of the CoNiCrAlY powder and resulting CGDS coatings demonstrated the occurrence of microstructural changes during the deposition process. Evidence of grain refinement of the initially large γ-matrix grains as well as dissolution of the fine β-phase precipitates was observed. Such transformations of the deposited material's microstructure were attributed to the intense plastic deformation resulting from the high-velocity impact of the sprayed particles. These findings contradict the generally accepted theory that the CGDS process does not lead to changes in the deposited material's microstructure. Although transformations in microstructure due to exposure to high temperatures are avoided, the CGDS process may still introduce microstructural changes by means of severe plastic deformation. Future work should be carried out to quantify the effects of such microstructural evolutions and investigate their influence on modelling work such as predicted critical velocities.

## Acknowledgement

The authors would like to acknowledge M. Brochu from McGill University for his assistance with the cryomilling process and equipment.

## References

[1] Alkhimov, Kosarev, Papyrin & Al, “Gas dynamic method for applying coating”, US patent 5 302 414, 12/04/1994.
[2] E. Irissou, J.-G. Legoux, A.N. Ryabinin, B. Jodoin, C. Moreau, “Review on Cold Spray Process and Technology: Part 1 — Intellectual Property, J. Therm. Spray Technol. (in press).
[3] L. Ajdelsztajn, B. Jodoin, G.E. Kim, J.M. Schoenung, J. Mondoux, Metall. Mater. Trans., A 36 (3) (2005) 657–666.
[4] H.J. Kim, C.H. Lee, S.Y. Hwang, Surf. Coat. Technol. 191 (2005) 335–340.
[5] J. Pattison, S. Celotto, R. Morgan, M. bray, W. O'Neill, Int. J. Mach. Tools Manuf. 47 (2007) 627–634.
[6] W. Kroemmer, P. Heinrich, Proceedings of the 2006 International Thermal Spray Conference, Seattle, Washington, USA, May 15–18, 2006.
[7] D. Grasme, in: P. Heinrich (Ed.), Proc. 6 Kolloqium Hochgeschwindigkeits-Flammspritzen (Unterschleiβheim, Germany), 2003, pp. 119–122, Gemeinschaft Thermisches Spritzen e.V.
[8] F. Gärtner, T. Stoltenhoff, T. Schmidt, H. Kreye, J. Therm. Spray Technol. 15 (2) (2006) 223–232.
[9] M. Grujicic, J.R. Saylor, D.E. Beasley, W.S. DeRosset, D. Helfritch, Appl. Surf. Sci. 219 (2003) 211–227.
[10] T.H. Van-Steenkiste, J.R. Smith, R.E. Teets, Surf. Coat. Technol. 154 (2002) 237–252.
[11] T. Stoltenhoff, C. Borchers, F. Gärtner, H. Kreye, Surf. Coat. Technol. 200 (2006) 4947–4960.
[12] R.S. Lima, A. Kucuk, C.C. Berndt, J. Karthikeyan, C.M. Kay, J. Lindemann, J. Mater. Sci. Lett. 21 (2002) 1687–1689.
[13] C.-J. Li, W.Y. Li, Y.Y. Wang, Surf. Coat. Technol. 198 (2005) 469–473.
[14] X.J. Ning, J.H. Jang, H.J. Kim, C.J. Li, C. Lee, Surf. Coat. Technol. 202 (2008) 1681–1687.
[15] L. Ajdelsztajn, A. Zuniga, B. Jodoin, E.J. Lavernia, Surf. Coat. Technol. 201 (2006) 2109–2116.
[16] P. Richer, B. Jodoin, L. Ajdelsztajn, E.J. Lavernia, J. Therm. Spray Technol. 15 (2) (2006) 246–254.
[17] L. Ajdelsztajn, B. Jodoin, J.M. Schoenung, Surf. Coat. Technol. 201 (2006) 1166–1172.
[18] L. Ajdelsztajn, B. Jodoin, P. Richer, E. Sansoucy, E.J. Lavernia, J. Therm. Spray Technol. 15 (4) (2006) 495–500.
[19] C.J. Li, G.J. Yang, P.H. Gao, J. Ma, Y.Y. Wang, C.X. Li, J. Therm. Spray Technol. 16 (5–6) (2007) 1011–1020.
[20] E. Sansoucy, P. Marcoux, L. Ajdelsztajn, B. Jodoin, Surf. Coat. Technol. 202 (2008) 3988–3996.
[21] R.C. Dykhuizen, M.F. Smith, D.L. Gilmore, R.A. Neiser, X. Jiand, S. Sampath, J. Therm. Spray Technol. 8 (4) (1999) 559–564.
[22] B. Jodoin, L. Ajdelsztajn, E. Sansoucy, A. Zuniga, P. Richer, E.J. Lavernia, Surf. Coat. Technol. 201 (2006) 3422–3429.
[23] T. Schmidt, F. Gärtner, H. Assadi, H. Kreye, Acta Mater. 54 (2006) 729–742.
[24] T.W. Wright, Int. J. Plast. 8 (5) (1992) 583–602.
[25] H. Assadi, F. Gärtner, T. Stoltenhoff, H. Kreye, Acta Mater. 51 (2003) 4379–4394.
[26] M. Grujicic, C.L. Zhao, W.S. DeRosset, D. Helfritch, Mater. Des. 25 (2004) 681–688.
[27] P.K. Wright, A.G. Evans, Curr. Opin. Solid State Mater. Sci. 4 (3) (1998) 255–265.
[28] K. Balani, A. Agarwal, S. Seal, J. Karthikeyan, Scr. Mater. 53 (2005) 845–850.
[29] M. Cohen, B.H. Kear, R. Mehrabian, in: R. Mehrabian, B.H. Kear, M. Cohen (Eds.), Rapid Solidification Processing: Principles and Technology II, Claitor, Baton Rouge, LA, 1980, p. 1.
[30] B. Jodoin, J. Therm. Spray Technol. 11 (4) (2002) 496–507.
[31] A.V. Korznikov, Y.V. Ivanisenko, D.V. Laptionok, I.M. Safarov, V.P. Pilyugin, R.Z. Valiev, NanoStruct. Mater. 4 (2) (1994) 157–164.
[32] Z. Horita, M. Furukawa, M. Nemoto, T.G. Langdon, Mater. Sci. Technol. 16 (11–12) (2000) 1239–1245.
[33] C. Suryanarayana, Int. Mater. Rev. 40 (1995) 41–64.
[34] R.Z. Valiev, R.K. Islamgaliev, I.V. Alexandrov, Prog. Mater. Sci. 45 (2000) 103–189.
[35] S.C. Tjong, H. Chen, Mater. Sci. Eng. R 45 (2004) 1–88.
[36] C. Suryanarayana, Prog. Mater. Sci. 46 (2001) 1–184.
[37] H. Bukker, G.F. Zhou, H. Yung, Prog. Mater. Sci. 39 (1995) 159–241.
[38] P.I. Loeff, A. Weeber, A.R. Miedema, J. Less-Common Met. 140 (1988) 299–305.